Space-charge-limited current flow in gallium nitride thin films

J. C. Vesely,* M. Shatzkes, and P. J. Burkhardt
IBM System Products Division, East Fishkill Technology Laboratory, Hopewell Junction, New York 12533
(Received 24 April 1973)

Polycrystalline gallium nitride (GaN) thin films, 1–5 μ thick, were deposited on degenerate silicon (Si) substrates by reactive rf sputtering at 45 °C. The resulting electrical characteristics are interpreted in terms of space-charge-limited current flow in the presence of two discrete trap levels. Analysis of the data indicates an equilibrium electron concentration of 5.2×10^{3}–7.8×10^{4} cm^{-3}, carrier mobility of 330 cm^2/V sec, and density of traps located 0.81 and 0.39 eV below the conduction band edge of 3.7×10^{14} and 1.9×10^{19} cm^{-3}, respectively. The effect of post-heat treatments in a continuous nitrogen gas flow is shown to decrease the carrier mobility and increase the concentration of shallow traps while maintaining the density of the deeper traps approximately constant. At large electric fields ($E>4\times10^{5}$ V/cm), a hot-electron effect is shown to be dominant.

I. INTRODUCTION

The III-V compound gallium nitride has been the subject of recent investigations because of its potential application in spontaneous- and stimulated-light-emission devices and as an insulating medium. GaN was demonstrated to crystallize in the hexagonal wurtzite structure and have a direct energy band gap of 3.39 eV.[1] It has been grown in monocrystalline needles by reacting molten gallium with ammonia,[2] and deposited epitaxially on a variety of substrates, most commonly Al_2O_3, via vapor transport,[1,3] solution growth,[4] and reactive evaporation.[5] The attainment of single-crystalline material necessitated the employment of relatively high growth temperatures [(850–1150) °C], and always resulted in n-type GaN with room-temperature electron concentrations and carrier mobilities of 10^{19} cm^{-3} and 85–150 cm^2/V sec, respectively. The inability to detect foreign impurities in such large concentrations resulted in the assumption that native donor defects (nitrogen vacancies or gallium interstitials) are the dominant donor species. Recently, GaN epitaxially grown at 1050 °C by vapor transport was reported to have a lower electron concentration of $(1–2)\times10^{17}$ cm^{-3} with $\mu = 400$ cm^2/V sec.[6]

p-type GaN has not yet been convincingly produced and the question whether type conversion is possible remains unanswered. However, the introduction of group-II or -IV acceptor impurities during vapor deposition resulted in high-resistivity material with values as great as 5×10^{8} Ω cm being observed.[7] High-resistivity (10^{6}-Ω cm) single-crystalline GaN has also been produced without resorting to the introduction of compensating impurities by the lower temperature (400–900 °C) process of decomposition of the gallium tribromide-ammonia complex.[8] Polycrystalline GaN, grown by reactive evaporation when the substrate was maintained at a temperature below 550 °C[5] and by reactive rf sputtering,[9] also yielded low-conductive thin films.

The electrical properties of polycrystalline gallium-nitride thin films fabricated by reactive rf sputtering are described. Interpretation of the observed current-voltage characteristics in terms of space-charge-limited current flow permitted calculation of the thermal-equilibrium electron concentration, carrier mobility, and density and energy location within the bandgap of the effective traps. Evidence for the existence of two discrete trap levels is presented, a situation not often encountered in other materials where space-charge-limited (SCL) current-flow mechanisms have been identified.[10] In large electric fields ($E>4\times10^{5}$ V/cm), the disagreement between the observed I-V characteristics and those of the expected square-law regime is found consistent with the introduction of a hot-electron effect.

II. EXPERIMENTAL

The method employed in the deposition of GaN was essentially that of Hovel and Cuomo.[9] The material was deposited on degenerate Si substrates, (111) orientation, by rf sputtering of a gallium target in the presence of nitrogen. The target consisted of a molybdenum disk coated with 99.999%-pure Ga and attached to a water-cooled cathode assembly. Prior to the introduction of nitrogen, a pressure of less than 10^{-7} Torr was attained while the substrate was maintained at the growth temperature of 45 °C. Nitrogen was purified initially by passage through a titanium sublimation pump and introduced into the chamber at a pressure of 3×10^{-2} Torr. During deposition, a frequency of 13.56 MHz was employed with a total

power input of 300 W. These conditions resulted in a growth rate of approximately 300 Å/min.

The thickness of the resulting depositions ranged from 1 to 5 μ as measured by the Taylor-Hobson taly-surf mechanical-stylus technique. The layers could be etched readily in concentrated phosphoric acid at 95 °C at a rate of 1600 Å/min. Measurement of the refractive index at a wavelength of 5461 Å yielded 2.44, which compares with a value of 2.397 ($\lambda = 5461$ Å) obtained on single-crystalline GaN grown by vapor transport.[11] Low-angle Laue x-ray measurements indicated the layers to be polycrystalline with crystallite sizes of 200–500 Å and having a (001) preferred orientation.

Contacts, 2×10^{-3} cm^2 in area, were constructed on the exposed GaN by evaporating aluminum or rf-sputtering indium nitride through a metal mask. InN films are highly conductive with electron concentrations and Hall mobilities of 10^{19} cm^{-3} and 250 cm^2/V sec, respectively.[9] A back-Al contact was also evaporated on the Si substrate to facilitate electrical measurements.

The electrical characteristics were obtained by a standard I-V measurement circuit. At low current levels, a Keithley Model 416 high-speed picoammeter was employed. All measurements above room temperature were conducted in a hot stage and in the presence of a continuous nitrogen gas flow.

III. THEORY OF SPACE-CHARGE-LIMITED CURRENT FLOW IN INSULATORS

The theory of space-charge-limited current flow in insulators has been considered in detail by Lampert and Mark[10] for a variety of trap distributions. In this section, the theory is extended to include the case of an insulator with two sets of traps. The basic assumptions that, (i) the cathode is capable of supplying any required current-injection level with a negligible fraction of the applied potential absorbed across the contact region, i.e., electric field at the cathode is approximately zero, (ii) the contribution of diffusion currents are negligible, (iii) carrier mobility is field independent in the voltage range considered, and (iv) the statistics of trap occupancy (satisfactorily obtained by employment of the quasi-Fermi concept) are all assumed valid. In addition, the traps are assumed to be discrete and not distributed in energy and characterized by concentrations and energy levels of N_{t_S}, N_{t_D} and E_{t_S}, $E_{t_D}(E_{t_S} > E_{t_D})$, respectively. The majority carriers are assumed to be electrons and all energies are defined with respect to the conduction-band edge which by convention is at zero energy. Employing the simplified regional-approximation method,[10] the obtained volt-ampere characteristics are shown in Fig. 1, with the relevant equations (T1)–(T28) summarized in Table I. The sharp transitions of Fig. 1 are a result of approximations in the method and would not be observed experimentally.

When the equilibrium Fermi level E_{F_0} is below both trap levels ($E_{t_S} > E_{t_D} > E_{F_0}$), the characteristic displays an Ohmic region plus three distinct square-law regions (solid curve, Fig. 1) associated with the deeper traps, shallow traps, and trap-free regime as given by Eqs. (T1)–(T7). These equations are only valid when $\theta_S \gg \theta_D$. The more general situation where this condition need not apply has been previously considered by English and Drews.[12] At large fields, the I-V characteristic will merge with the trap-free square law (J_{TF}), which is the largest one-carrier injec-

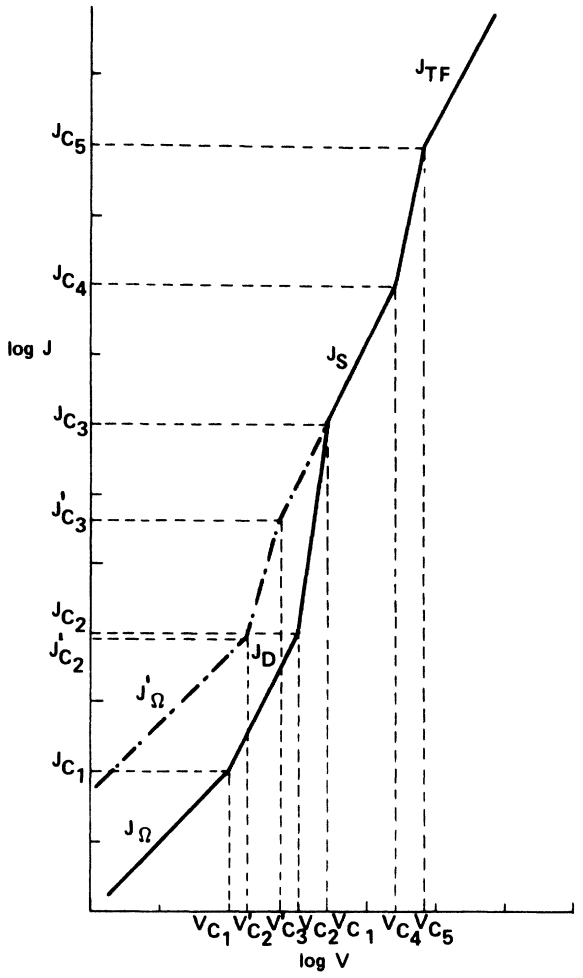

FIG. 1. Theoretical volt-ampere characteristics for space-charge-limited current flow in the presence of two discrete trap levels. Solid curve: $E_{t_S} > E_{t_D} > E_{F_0}$, $(E_{t_D} - E_{F_0})/kT > 1$; dashed curve: $E_{t_S} > E_{F_0} > E_{t_D}$, $(E_{t_D} - E_{F_0})/kT < 1$.

tion current the insulator is capable of carrying. If the low-frequency dielectric constant is known, voltages V_{C2} (assuming $\theta_D \ll \theta_S$) and V_{C4} in combination with Eqs. (T11) and (T15) will yield N_{t_D} and N_{t_S} directly. In turn, if the effective density of states in the conduction band N_c, carrier mobility μ, dielectric constant ϵ, and the trap-degeneracy factor g are known, the energy location of the traps within the band gap can be obtained via Eqs. (T3)–(T6).

For comparison, the situation when the equilibrium Fermi level lies between the two trap levels ($E_{t_S} > E'_{F_0} > E_{t_D}$) is also included (dashed curve, Fig. 1; Eqs. (T18)–(T20), Table I). This characteristic was obtained by assuming that all parameters of the above case remain unchanged with the exception that the equilibrium concentration is increased. This condition may arise because of a slight alteration in the concentration of compensating acceptor centers. The deep-trap square-law region is no longer present, with the characteristic going from Ohmic to transition to shallow-trap square-law region as the bias is increased. Only a minimum concentration of deeper traps (those unoccupied by electrons at thermal equilibrium) can be determined from V'_{C2} and Eq. (T22). It is of interest to note that the current density at which the first transition region is entered remains approximately unchanged for both cases ($J_{C2} \approx J'_{C2}$). For voltages greater than V_{C3}, the two characteristics are identical.

For a variety of reasons, including the inability

TABLE I. Fundamental parameters and transitions in volt-ampere characteristics for space-charge-limited current flow in the presence of two discrete trap levels for an insulator of thickness L.

I. $E_{t_S} > E_{t_D} > E_{F_0}$; $(E_{t_D} - E_{F_0})/kT > 1$

$J_\Omega = n_0 q\mu V/L$	(T1),	$n_0 = N_c e^{E_{F_0}/kT}$	(T2)
$J_D = 9\Theta_D \epsilon \mu V^2/8L^3$	(T3),	$\Theta_D = (N_c/gN_{t_D}) e^{E_{t_D}/kT}$	(T4)
$J_S = 9\theta_S \epsilon \mu V^2/8L^3$	(T5),	$\theta_S = (N_c/gN_{t_S}) e^{E_{t_S}/kT}$	(T6)
$J_{TF} = 9\epsilon \mu V^2/8L^3$	(T7),		

Transitions

$J_{C1} = 8q^2 n_0^2 \mu L/9\Theta_D \epsilon$	(T8),	$V_{C1} = 8q n_0 L^2/9\Theta_D \epsilon$	(T9)
$J_{C2} = \Theta_D q^2 \mu N_{t_D}^2 L/\epsilon (1 - \Theta_D/2\theta_S)$	(T10),	$V_{C2} = qN_{t_D} L^2/2\epsilon (1 - \Theta_D/2\theta_S)^{1/2}$	(T11)
$J_{C3} = 2\theta_S q^2 \mu N_{t_D}^2 L/\epsilon$	(T12),	$V_{C3} = 4qN_{t_D} L^2/3\epsilon$	(T13)
$J_{C4} = \theta_S q^2 \mu N_{t_S}^2 L/\epsilon$	(T14),	$V_{C4} = qN_{t_S} L^2/2\epsilon$	(T15)
$J_{C5} = 2q^2 \mu N_{t_S}^2 L/\epsilon$	(T16),	$V_{C5} = 4qN_{t_S} L^2/3\epsilon$	(T17)

II. $E_{t_S} > E'_{F_0} > E_{t_D}$; $(E_{t_D} - E'_{F_0})/kT < 1$

$J'_\Omega = n'_0 q \mu V/L$	(T18),	$n'_0 = N_c e^{(E'_{F_0}/kT)}$	(T19)
$J'_\Omega/J_\Omega = e^{(E'_{F_0} - E_{F_0})/kT}$	(T20),	$\theta_S = (N_c/gN_{t_S}) e^{E_{t_S}/kT}$	
$J_S = 9\theta_S \epsilon \mu V^2/8L^3$		$J_{TF} = 9\epsilon \mu V^2/8L^3$	

Transitions

$J'_{C2} = n'_0 q^2 \mu p_{D,0} L/\epsilon$	(T21),	$V'_{C2} = q p_{D,0} L^2/2\epsilon$	(T22)
$V'_{C2}/V_{C2} = p_{D,0}/N_{t_D} = (1/g) e^{(E_{t_D} - E'_{F_0})/kT}$			(T23)
$J'_{C2}/J_{C2} = p_{D,0} n'_0/\Theta_D N_{t_D}^2 = 1$		if $\Theta_D \ll \theta_S$	(T24)
$J'_{C3} = 2\theta_S q^2 \mu_{D,0}^2 L/\epsilon$	(T25),	$V'_{C3} = 4q p_{D,0} L^2/3\epsilon$	(T26)
$V'_{C3}/V_{C3} = p_{D,0}/N_{t_D} = (1/g) e^{(E_{t_D} - E'_{F_0})/kT}$			(T27)
$J'_{C3}/J_{C3} = p_{D,0}^2/N_{t_D}^2 = (1/g)^2 e^{2(E_{t_D} - E'_{F_0})/kT}$			(T28)
$J_{C4} = \theta_S q^2 \mu N_{t_S}^2 L/\epsilon$		$V_{C4} = qN_{t_S} L^2/2\epsilon$	
$J_{C5} = 2q^2 \mu N_{t_S}^2 L/\epsilon$		$V_{C5} = 4qN_{t_S} L^2/3\epsilon$	

to detect low current levels, electrical breakdown of insulators at high fields and the absence of two-trap levels, the complete characteristics of Fig. 1 have not been observed experimentally. However, space-charge-limited current investigations on a number of different insulators, most notably the II-VI compounds, have yielded detailed characterizations of these materials which have been confirmed by independent experiments.[10,13-15]

IV. EXPERIMENTAL RESULTS

Figure 2 shows the dc steady-state I-V characteristics obtained for samples 1.36 and 2.4 μ in thickness. The Al pad was biased positively with respect to the degenerate p-type silicon substrate and the current rapidly stabilized at a given voltage with little evidence of hysteresis. The curves were also found essentially independent of bias polarity, contact material (Al or InN), and substrate type (p^+ or n^+).

The similarity between the experimental curves and those of Fig. 1 are obvious. The thicker sample displayed the following regions: Ohmic, square law, transition, and square law and transition. The 1.36-μ sample had the first square-law region omitted, but its conductivity in the Ohmic region is increased considerably. For fields greater than 2×10^6 V/cm, the samples underwent an electrical breakdown which resulted in a short. Therefore, it is questionable whether the second square law is a trap-free region followed by electrical breakdown, or whether it is a shallower-trap square law proceeded by a transition into an unobservable trap-free region.

For the 2.4-μ sample, $\theta_D\mu$ and $\theta_S\mu$ products of 3.8×10^{-8} and 8.6×10^{-6} cm^2/V sec were calculated from Eqs. (T3) and (T5). These values compare to $\theta\mu$ products of 6.2×10^{-3} [16] and 3.4×10^{-1} [8] cm^2/V sec calculated from square-law regions previously observed in the I-V characteristics of high-resistivity single-crystalline GaN thin films. If the upper square-law region is a true trap-free

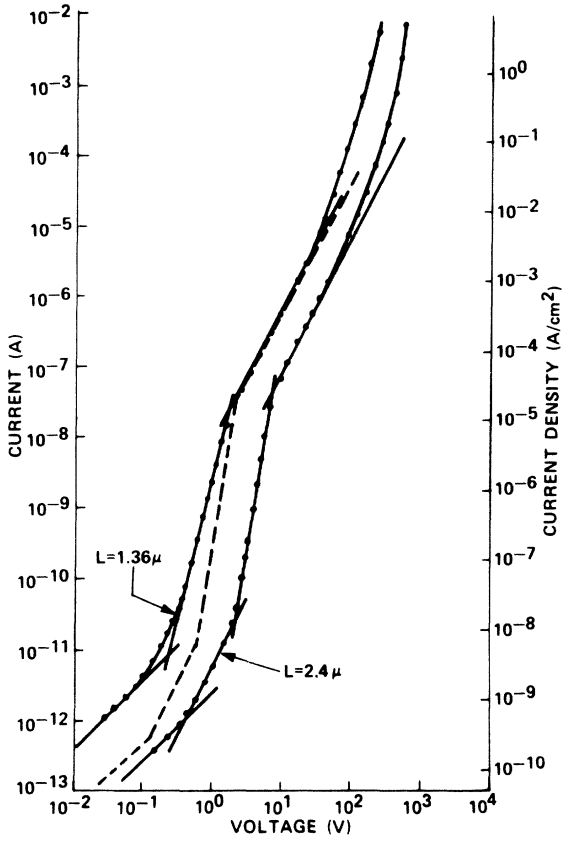

FIG. 2. Experimental volt-ampere characteristics observed for samples 1.36 and 2.4 μ thick. Dashed curve—expected volt-ampere characteristic for 1.36 μ sample if all parameters calculated for 2.4 μ sample were assumed valid. Al pad biased positive with respect to p^+ Si substrate.

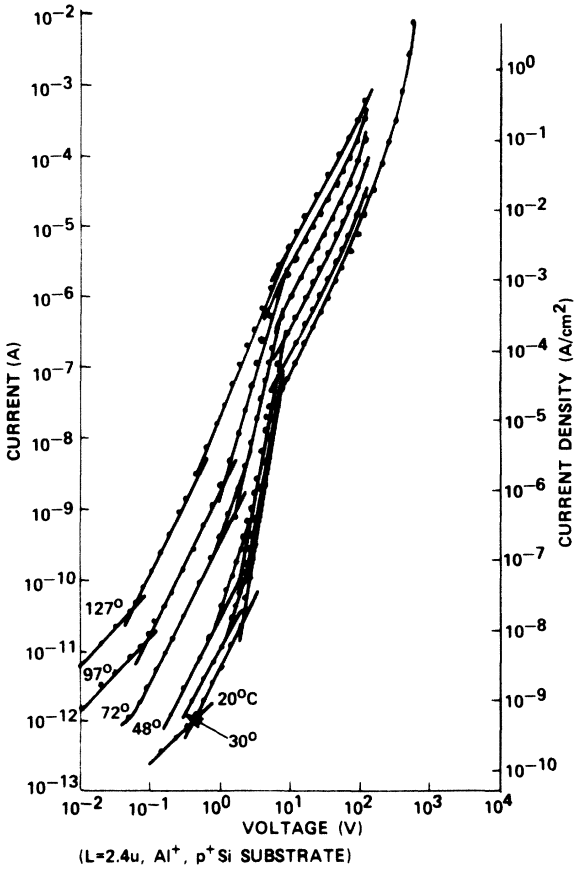

FIG. 3. Volt-ampere characteristics of 2.4-μ sample as a function of temperature. Al pad biased positive with respect to p^+ Si substrate.

condition ($\theta = 1$), a carrier mobility of 8.6×10^{-6} cm^2/V sec is required, an exceedingly small value. Assuming θ is equal to unity in this region, Eq. (T7) predicts that a temperature-variation experiment would display only the variation in mobility, which is expected to be small and inversely proportional to temperature.

Figure 3 shows a series of I-V curves as a function of temperature in the range of 20–127 °C. Above approximately 150 °C, the samples underwent a transformation which drastically altered their I-V characteristics when returned to room temperature. The two square-law regions are present in all cases, with the $\theta\mu$ product of the first increasing at a faster rate than that of the second. Since the variation with temperature of the $\theta\mu$ product for the upper square law cannot be explained in terms of mobility changes, it is concluded to be due to a shallower trap and not characteristic of a trap-free region.

For the sample 2.4 μ thick, and employing the previously published low-frequency dielectric constant of GaN to be 9.8,[17] $V_{C2} = 2$ V and $V_{C4} = 100$ V in combination with Eqs. (T11) ($\theta_D/2\theta_S = 2.2 \times 10^{-3}$) and (T15) yields values for N_{t_D} and N_{t_S} of 3.8×10^{14} and 1.9×10^{16} cm^{-3}, respectively. The latter concentration will be shown to be in considerable error because the observed transition at 100 V is not a true space-charge-limited transition. Figure 4 shows a plot of $\log_{10} I$ vs $1/T$ for a number of bias voltages. Two distinct activation energies are present with values of 0.39 and 0.81 eV and corresponding to E_{t_S} and E_{t_D}, respectively.

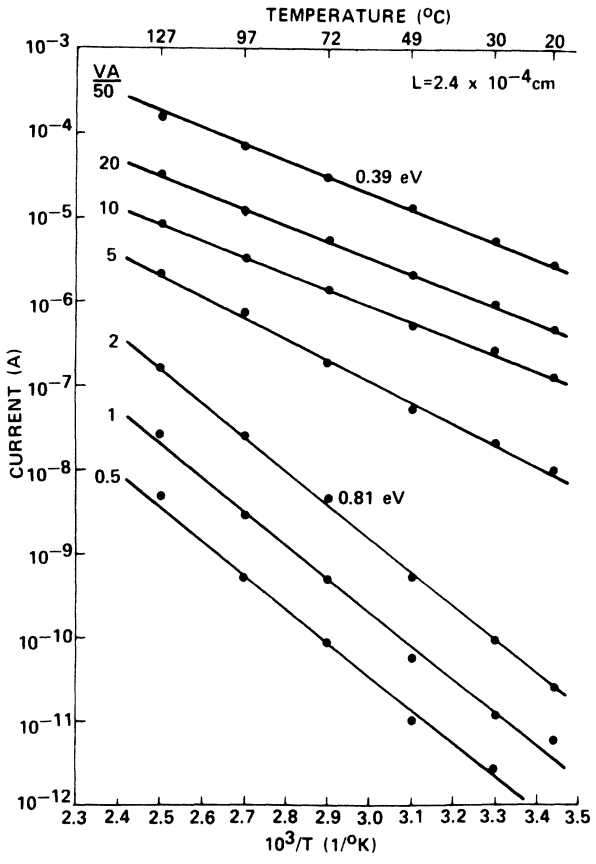

FIG. 4. Data of Fig. 3 plotted as $\log_{10} I$ vs $1/T$ with V applied constant.

Assuming an effective density of states in the conduction band of 3.1×10^{18} cm^{-3} at 300 °K,[18] and a degeneracy factor of 2, a value for Θ_D of 1.15×10^{-10} cm^2/V sec was calculated via Eq. (T4). Since $\Theta_D\mu = 3.8 \times 10^{-8}$ cm^2/V sec, the carrier mobility is estimated to be 330 cm^2/V sec, a value previously observed in single-crystalline material by Hall measurement techniques.[6] As pointed out by Bube,[14] the intercept of a θ vs $1/T$ plot at $1/T = 0$ equals N_c/gN_t, and provides an independent means of checking the trap concentration obtained from transition voltages. This construction was also found consistent with an N_{t_D} of 3.8×10^{14} cm^{-3}.

With the availability of both μ and Θ_D, either Eq. (T1) or (T9) can determine the equilibrium electron concentration. Both calculations resulted in a value for n_0 of 5.2×10^3 cm^{-3}, which corresponds to a resistivity of 3.6×10^{12} Ω cm. From Eq. (T2), the equilibrium Fermi level lies 0.88 eV below the conduction-band edge and approximately $3kT$ below E_{t_D}.

It can now be demonstrated that the departure from the shallow-trap square law, observed at 100 V, cannot be accredited to a transition into a trap-free region. We will show, below, that this transition can be explained by a hot-electron effect. Taking the $\theta_S\mu$ product calculated from Eq. (T5) of 8.6×10^{-6} cm^2/V sec and a carrier mobility of 330 cm^2/V sec, Eq. (T6) yields a value for N_{t_S} of 1.9×10^{19} cm^{-3}, three orders of magnitude greater than the value that would be obtained by making

TABLE II. Summary of parameters calculated from volt-ampere characteristics of samples 1.36 and 2.4 μ thick.

L	(cm)	2.4×10^{-4}	1.36×10^{-4}
E_{F_0}	(eV)	−0.88	−0.81
n_0	(cm^{-3})	5.2×10^3	7.8×10^4
μ	(cm^2/V sec)	330	330
ρ	(Ω cm)	3.65×10^{12}	2.94×10^{11}
N_{t_D}	(cm^{-3})	3.7×10^{14}	4.2×10^{14} [a]
E_{t_D}	(eV)	−0.81	−0.81
Θ_D		1.14×10^{-10}	...
N_{t_S}	(cm^{-3})	1.9×10^{19}	1.9×10^{19}
E_{t_S}	(eV)	−0.39	−0.39
θ_S		2.58×10^{-8}	2.58×10^{-8}

[a] $p_{D,0} = N_{tD}/[1 + 8\, e^{(E_{F_0} - E_{t_D})/kT}] = 1.4 \times 10^{14}$.

the false assumption that the transition observed at 100 V corresponds to V_{C4}. The intercept of θ_S vs $1/T$ at $1/T = 0$ also yielded a larger value for N_{t_S} of 1.4×10^{19} cm^{-3}. The actual V_{C4} transition can be calculated by employing $N_{t_S} = 10^{19}$ cm^{-3} in combination with Eq. (T15) which results in a value of 10^5 V, a condition completely unattainable experimentally.

Figure 2 also shows the predicted characteristic (dashed curve) if the sample thickness was 1.36 μ and all of the parameters determined above were valid. The $\theta_S\mu$ product is observed to scale correctly with thickness, and since it is difficult to envision a mechanism whereby both μ and θ_S vary in such a manner as to maintain their product constant, it is concluded that $\mu = 330$ cm^2/V sec and $N_{t_S} = 1.9\times10^{19}$ cm^{-3} for the thinner sample. From Eq. (T22), $n_0' = 7.8\times10^4$ cm^{-3}, a factor of 15 greater than for the thicker sample. This change in the equilibrium electron concentration could be due to a slight decrease in the density of compensating acceptor centers. E_{F_0} for this sample is −0.81 eV,

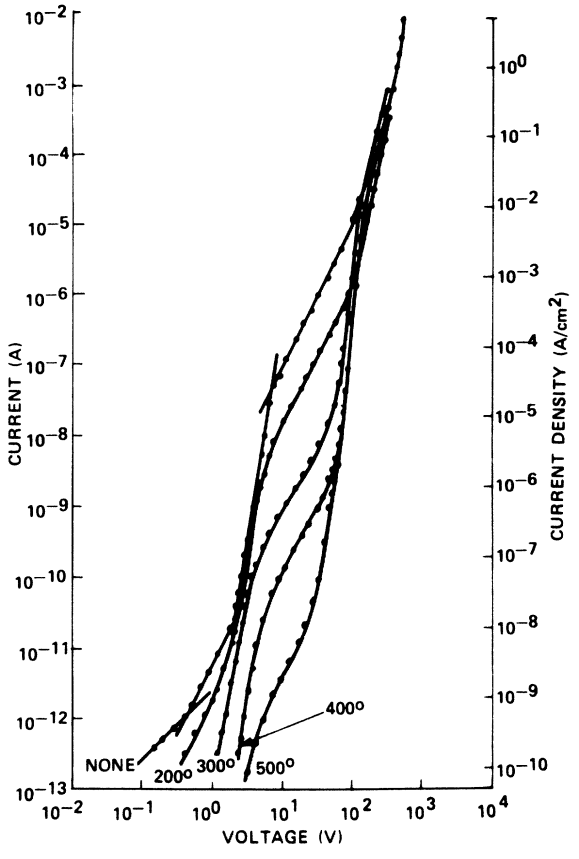

FIG. 5. Volt-ampere characteristics obtained at room temperature following post-heat treatments for 1 h in nitrogen gas. Al pas biased positive with respect to n^+ Si substrates, $L = 2.3$ μ.

placing it approximately at the deep-trap energy level and explains why the first square-law region was not observed. Equation (T22), with $V_{C2}' = 0.25$ V, yields a value for $p_{D,0}$ (deep traps unoccupied by an electron at thermal equilibrium) of 1.4×10^{14} cm^{-3}. Table II summarizes the parameters calculated from analysis of both samples.

As previously stated, samples treated above 150 °C displayed pronounced changes in their electrical characteristics. To elucidate more of this effect, samples were treated at elevated temperatures for 1 h in nitrogen gas flow, returned to room temperature and their I-V characteristics measured. Figure 5 shows the results of this experiment. Under optical microscopic examination, samples treated above 500 °C displayed excessive damage and were characterized by numerous cracks and bubbles, some of which had burst open. GaN is known to dissociate at temperatures of 600 °C, [19] and the formation and eventual eruption of the bubbles are believed to be a manifestation of the escaping nitrogen gas.

Examination of the electrical data indicates that transition V_{C3} remained approximately constant at 7 V for all of the treated samples, implying that N_{t_D} is constant and equal to approximately 3.7×10^{14} cm^{-3}. However, the drastic decrease in the $\theta_S\mu$ product as the annealing temperature was increased is evident, with the calculated products summarized in Table III. Since $\theta_S\mu$ is a decreasing function of annealing temperature, the carrier mobility is decreased and/or the concentration of shallow traps is increased. That μ is decreasing with increasing annealing temperature is evident from the deep-trap square-law region. Since N_{t_D}, and consequently Θ_D, are constant, the variation in the $\theta_D\mu$ product only reflects the change in carrier mobility. For example, analysis of the electrical characteristics for the film annealed at 200 °C yielded $\mu = 110$ cm^2/V sec, with N_{t_D} and N_{t_S} equal to 3.7×10^{14} and 4.9×10^{19} cm^{-3}, respectively. A complete analysis for the other treated samples was not possible because of the lack of suitable

TABLE III. Calculated $\theta_S\mu$ products from Fig. 5 for the various post-heat treatments.

Annealing temperature[a] (°C)	$\mu\theta_{S_2}$ product (cm^2/V sec)
none	8.6×10^{-6}
200	1.1×10^{-6}
300	6.4×10^{-8}
400	8.6×10^{-9}
500	3.0×10^{-10}

[a] All treatments of 1-h duration in N_2 gas.

data. However, it can be concluded that the effect of high-temperature heat treatment is to decrease the carrier mobility while increasing the concentration of shallow traps and having little or no effect on the concentration of deep traps.

V. DISCUSSION

The major implication of the experimental data and subsequent analysis in terms of space-charge-limited current flow is the detection of two discrete trap levels 0.81 and 0.39 eV below the conduction-band edge with concentrations of 3.7×10^{14} and 1.9×10^{19} cm^{-3}, respectively. The identity of these centers cannot be deduced from the experimental data, since the only criterion for a trap in space-charged-limited current-flow theory is that it be any localized electronic defect state whose electron occupation is given by the Fermi-Dirac function. Hence, the centers could be donor states which are positively charged when unoccupied by an electron, or electron traps which are neutral when not occupied. It is obvious that if the centers are donors, and since the equilibrium Fermi level is located 0.8–0.9 eV below the conduction-band edge, the material is almost totally compensated by deeper-lying acceptor centers. This is not an unusual phenomena, and has been observed in CdS,[20] GaAs[21] and a wide variety of other compound semiconductors.

Previous experimentally observed electronic defect states in GaN are very limited. Since most undoped single-crystalline material is heavily n type with electron concentrations of 10^{19} cm^{-3},[1-5] carrier freeze out is not possible and consequently an activation energy for the responsible donor center could not be obtained via low-temperature Hall measurements. However, examination of the near ultraviolet photoluminescence observed at low temperatures has been interpreted in terms of a radiative transition between a donor-acceptor pair, with the donor level estimated to be 0.042 eV below E_c and the acceptor center 0.2 eV above the valence-band edge.[17] It should be noted that the only defect states capable of detection in space-charge-limited current-flow experiments are those in which the quasi-Fermi level can be swept through via variation of the current injection level. In the present study, this corresponds to a bandwidth approximately 0.4 to 0.9 eV below the conduction-band edge, consequently, any defect states lying outside of this region will remain undetected.

Chu[8] observed space-charge-limited current flow in nonintentionally doped, high-resistivity GaN, and by plotting $\ln I$ vs $1/T$, concluded that a deep-lying impurity at approximately 1.1 eV was dominant. Pankove *et al.*,[16] employing the same technique, observed a 0.13-eV activation energy above room temperature for Zn-doped single-crystal GaN in the region where the voltage was quadratically dependent on current. Although neither of the above activation energies correspond to those observed in this study, the existence of deep-lying electronic defect states in both monocrystalline and polycrystalline high-resistivity GaN is evident. Apparently, the energy level and density of these traps are a critical function of deposition conditions. This statement is supported by the experimental evidence that annealing of the samples increased the concentration of shallow traps located 0.39 eV below E_c, and further suggests that the centers are possibly due either to large-scale disorders, such as crystal imperfections caused by internal stress, or native point defects which are deviations from stoichiometry.

Observations of a carrier mobility in polycrystalline GaN comparable to that measured in single-crystal material[6] would at first appear contradictory. However, as emphasized by Mott and Davis,[22] the mobility obtained via analysis of space-charge-limited current flow is the microscopic or conductivity mobility, with the drift or effective mobility being given by the $\theta\mu$ product. In the present study, this would correspond to an effective mobility of 8.6×10^{-6} $cm^2/V\,sec$ for fields greater than 4×10^4 V/cm.

The present lack of knowledge concerning the fundamental parameters of GaN does not permit calculation of an expected mobility due only to lattice scattering. However, employing the Conwell-Weisskopf formula for scattering by ionized impurities[23] and assuming that traps N_{t_S} are donors and completely compensated, a mobility of 45 $cm^2/V\,sec$ is calculated, a value seven times lower than observed. The possibility of donor-acceptor pairs acting as dipoles which are known to scatter far less effectively than an equal number of isolated ionized impurities[24] could account for this discrepancy. The observed inverse proportionality of carrier mobility with trap concentration N_{t_S} resulting from the heat-treatment experiments ($N_{t_{S2}}/N_{t_{S1}}=2.6$, $\mu_1/\mu_2=3.0$ where subscripts 1 and 2 denote no annealing and 200 °C annealing, respectively), also indicates that an ionized impurity-scattering mechanism is dominant and that shallow traps are donors, and consequently almost totally compensated by deep-lying acceptors.

As previously demonstrated, the transition from the shallow-trap square law observed at 100 V ($L=2.4$ μ) is not a space-charge-limited current transition into a trap-free region, which would theoretically occur at a much larger voltage, but due to another effect. This rapid increase in current can be understood in terms of a model intro-

duced by Frohlich[25] to explain dielectric breakdown. The invoking of this mechanism requires that it successfully accounts for the electrical breakdown observed at fields of approximately 2×10^6 V/cm.[26]

In this model there are, in addition to the levels located at 0.39 and 0.81 eV, numerous electron traps distributed over a range ΔV below the conduction-band edge. A temperature T_e, different from the lattice temperature T, can be assigned to the electrons which, according to Frohlich, is given by,

$$1/kT_e = 1/kT - (E/E_B)^2\ 1/\Delta V, \tag{1}$$

where E is the electric field and E_B the breakdown field.

In the shallow-trap square-law region, Poisson's equation can be written approximately as

$$\frac{dE}{dx} = \frac{qn}{\epsilon\theta_S'} = \frac{J}{\epsilon\mu\theta_S' E}, \tag{2}$$

since neglecting diffusion currents $J = q\mu nE$ = constant. Now, θ_S' is as given in Eq. (T6) except that the electron temperature T_e is used in place of the lattice temperature. Thus,

$$\begin{aligned} E_0^2 &= E_B^2 \Delta V/(-E_{t_S}), \\ \theta_S' &= \theta_S\, e^{(E/E_0)^2}, \end{aligned} \tag{3}$$

where

$$\theta_S = (N_c/gN_{t_S})\, e^{E_{t_S}/kT}.$$

Using Eq. (3) for θ_S' in Eq. (2), assuming zero cathode field and integrating, yields an equation relating the current density to the field at the anode E_A,

$$(J/J_{\mathrm{SCL}}) = (4L^2E_0^2/9V^2)[\, e^{(E_A/E_0)^2} - 1], \tag{4}$$

where

$$J_{\mathrm{SCL}} = \tfrac{9}{8}\epsilon\mu\theta_S V^2/L^3.$$

The applied potential is also related to the anode field through

$$V = \int_0^{E_A} E\,dE \Big/ \frac{dE}{dx}, \tag{5}$$

which, with Eqs. (2) and (3), provides the relation

$$V = \frac{E_A L[\,1 - (E_0/E_A)D(x)]}{1 - e^{-(E_A/E_0)^2}}, \tag{6}$$

where $x = E_A/E_0$ and $D(x) = e^{-x^2}\int_0^x e^{y^2}\,dy$ which is the Dawson integral.[27]

Equation (4) in combination with Eq. (6) determines J as a function of applied voltage V. A comparison of the results predicted by this model with those experimentally observed are shown in Fig. 6. The parameters employed in the calculations were $E_B = 2\times10^6$ V/cm and $E_0 = 8.5\times10^5$ V/cm ($\Delta V = -0.07$ eV). The model correctly predicts the deviation from the shallow-trap square-law region and approximately reproduces the shape of the volt-ampere characteristics at larger fields. The steeply rising current with fields greater than 2×10^6 V/cm successfully predicts the eventual breakdown of the device. The data points shown at the largest currents (Fig. 6) correspond to those taken immediately preceding breakdown.

VI. CONCLUSIONS

An analysis of the volt-ampere characteristics of rf-sputtered GaN was made in terms of space-charge-limited current flow. A plot of $\ln I$ vs $1/T$ (V = constant) for each observed square-law region yielded the respective energy levels for two sets of discrete traps, while extrapolation of this construction to $1/T = 0$ yielded the trap concentrations which were found consistent with the various transition voltages. In addition, the conductivity mobility and equilibrium electron concentration

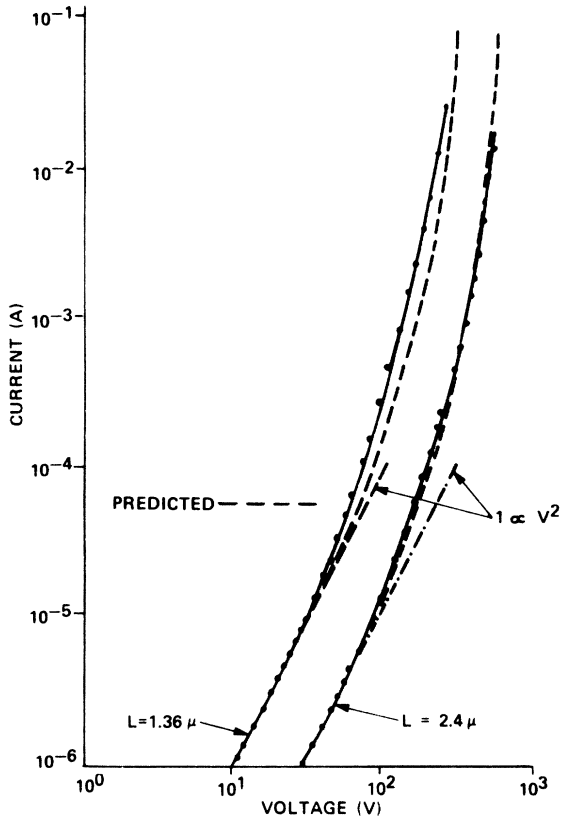

FIG. 6. Comparison of volt-ampere characteristics experimentally observed (solid curve) with those calculated by employing the hot-electron effect with $E_0 = 8.5\times10^5$ V/cm and $E_B = 2.0\times10^6$ V/cm (dashed curve). Al pad biased positive with respect to p^+ Si substrate.

were obtained. The rapid rising current with voltage at high fields was demonstrated not to be a true space-charge-limited transition, but rather due to a hot-electron effect, which successfully predicted the eventual breakdown of the device.

Consideration of the equilibrium Fermi level and calculated conductivity mobility indicated that the traps are probably donors which are almost totally compensated by acceptors, and partially, at least, associate to form donor-acceptor pairs and scatter carriers as dipoles. The effect of post-heat treatments was to decrease mobility and increase the concentration of shallow traps (and consequently, compensating acceptor centers), and are believed to be either a manifestation of crystallographic imperfections or native point defects.

ACKNOWLEDGMENTS

The authors wish to acknowledge the invaluable contributions to this work by L. Rothman and R. A. Carruthers for the film depositions and R. M. Anderson for x-ray crystallographic analysis. The many rewarding discussions with E. L. Boyd are gratefully appreciated.

---

*Present address: Texas Instruments Inc., Houston, Tex. 77001.

[1]H. P. Maruska and J. J. Tietjin, Appl. Phys. Lett. 15, 327 (1969).

[2]D. D. Manchon, Jr., A. S. Barker, Jr., P. J. Dean, and R. B. Zetterstrom, Solid State Commun. 8, 1227 (1970).

[3]D. K. Wickenden, K. R. Faulkner, R. W. Brander, and B. J. Isherwood, J. Cryst. Growth 9, 158 (1971).

[4]R. A. Logan and C. D. Thurmond, Bull. Am. Phys. Soc. 17, 233 (1972).

[5]B. B. Kosicki, and D. Kahng, J. Vac. Sci. Technol. 6, 593 (1969); B. B. Kosicki, R. J. Powell, and J. C. Burgiel, Appl. Phys. Lett. 24, 1421 (1970).

[6]M. Ilegems, J. Cryst. Growth, 13/14, 360 (1972).

[7]J. I. Pankove, E. A. Miller, and J. E. Berkeyheiser, J. Lumin. 5, 84 (1972).

[8]T. L. Chu, J. Electrochem. Soc. 118, 1200 (1971).

[9]H. J. Hovel and J. J. Cuomo, Appl. Phys. Lett. 20, 71 (1972).

[10]M. A. Lampert and P. Mark, *Current Injection in Solids* (Academic, New York, 1970).

[11]J. I. Pankove, J. E. Berkeyheiser, H. P. Maruska, and J. Wittke, Solid State Commun. 8, 1051 (1970).

[12]A. C. English and R. E. Drews, Sci. Electron. 9, 1 (1963).

[13]R. W. Smith and A. Rose, Phys. Rev. 97, 1531 (1955).

[14]R. H. Bube, J. Appl. Phys. 33, 1733 (1962).

[15]W. Ruppel, Helv. Phys. Acta. 31, 311 (1958).

[16]J. I. Pankove, E. A.Miller, and J. E. Berkeyheiser, RCA Rev. 32 , 383 (1971).

[17]R. Dingle and M. Ilegems, Solid State Commun. 9, 175 (1971).

[18]Calculated by assuming a scalar effective mass of 0.25 m (see Ref. 17).

[19]M. R. Lorenz and B. B. Binkowski, J. Electrochem. Soc. 109, 24 (1962).

[20]D. J. Page, A. A. Kayali, and G. T. Wright, Proc. Phys. Soc. Lond. B 80, 1133 (1962).

[21]J. W. Allen and R. J. Cherry, Nature (Lond.) 189, 297 (1961).

[22]N. F. Mott and E. A. Davis, *Electronic Processes in Non-Crystalline Materials* (Claredon, Oxford, 1971), p. 209.

[23]E. M. Conwell and V. F. Weisskopf, Phys. Rev. 77, 388 (1950).

[24]Y. Fukuda and M. Fukai, J. Phys. Soc. Jap. 23, 902 (1967); R. Stratton, J. Phys. Chem. Solids 23, 1011 (1962); A. Boardman, Proc. Phys. Soc. Lond. 85, 141 (1965).

[25]H. Frohlich, Proc. R. Soc. A 188, 521 (1947); J. J. O'Dwyer, J. Appl. Phys. 37, 599 (1966); J. C. Schug, A. C. Lilly, Jr., and D. A. Lowitz, Phys. Rev. B 1, 4811 (1970); J. Antula, J. Appl. Phys. 43, 4663 (1972).

[26]Different effects were considered to resolve a similar discrepancy on space-charge-limited current measurements in naphthalene and CdS monocrystals (J. Dresner, M. Campos, and R. A. Moreno, J. Appl. Phys. 44, 3708 (1973)). In our particular case, we prefer a hot-electron model for reasons to be indicated in the text. (i) The current as a function of voltage as derived from Eqs. (4) and (6) fit the experimental data over an extended range both before and after the apparent transition and scale properly with sample thickness (Fig. 6). (ii) It provides a consistent mechanism for both the steeply rising current and eventual breakdown.

[27]M. Abromowitz and I. A. Stegun, *Handbook of Mathematical Functions* (Dover, New York, 1963), p. 319.